Magnetic Resonance in Medicine 47:1052–1058 (2002)

Toward Direct Mapping of Neuronal Activity: MRI Detection of Ultraweak, Transient Magnetic Field Changes

Jerzy Bodurka[1*] and Peter A. Bandettini[1,2]

A novel method based on selective detection of rapidly changing ΔB_0 magnetic fields and suppression of slowly changing ΔB_0 fields is presented. The ultimate goal of this work is to present a method that may allow detection of transient and subtle changes in B_0 in cortical tissue associated with electrical currents produced by neuronal activity. The method involves the detection of NMR phase changes that occur during a single-shot spin-echo (SE) echo-planar sequence (EPI) echo time. SE EPI effectively rephases all changes in B_0 that occur on a time scale longer than the echo time (TE) and amplifies all ΔB_0 changes that occur during TE/2. The method was tested on a phantom that contains wires in which current can be modulated. The sensitivity and flexibility of the technique was demonstrated by modulation of the temporal position and duration of the stimuli-evoked transient magnetic field relative to the 180 RF pulse in the imaging sequence—requiring precise stimulus timing. Currently, with this method magnetic field changes as small as 2×10^{-10} T (200 pT) and lasting for 40 msec can be detected. Implications for direct mapping of brain neuronal activity with MRI are discussed. Magn Reson Med 47: 1052–1058, 2002. Published 2002 Wiley-Liss, Inc.†

Key words: magnetic field; magnetic phase; neuronal activity; MRI; brain mapping

In recent years there have been rapid advances in methods to map human brain activity. One of the most recently developed techniques, functional MRI (fMRI), is based on the sensitivity of MRI to oxygenation, flow, and perfusion changes concomitant with an increase in brain activation. The spatial and temporal resolutions of this technique are limited by cerebral neuronal-hemodynamic coupling precision, rather than physical limitations of the imaging methodology. Spatial resolutions on the order of 1 mm and temporal resolutions on the order of 1 sec have been achieved (1–5). Magnetoencephalography (MEG) and electroencephalography (EEG) allow measurement of brain electric activity with a temporal resolution on the order of milliseconds but lower spatial resolution (6–8). A significant effort has been made to combine information from these different modalities in order to obtain high spatial and temporal resolution maps of brain activation (9,10). An ultimate goal is the direct mapping of these dipole sources. In the study presented, we introduce and outline the feasibility of an MRI-based method to directly detect and map transient magnetic field changes corresponding to synchronous neuronal firing.

The well-understood sensitivity of MRI to magnetic field variations was first utilized about a decade ago to map electric current density in homogenous and heterogeneous media (11,12). The effects of externally applied small (~2 mA) electric current pulses has been shown to be detectable in the human body (13). The challenge of detecting neuronal currents resulting from brain activity is much more difficult, since these currents are approximately three orders of magnitude smaller, much more transient, and perhaps localized to a smaller region in space, than what has been detected previously using MRI. These ionic currents induce subtle and transient magnetic flux density (ΔB) changes, depending on their temporal and spatial coherence. The parallel to B_0 component of these fields (ΔB_0) alters the magnetic phase of surrounding water protons and thus influences the phase and/or magnitude of the MRI signal—depending on the size and geometry of the synchronous current sources.

Evoked or spontaneous magnetic fields (EMF or SMF) measured on the scalp (measurement distance $r_{MEG} \approx 2$–4 cm away from the current source) by MEG are on the order of a $\Delta B \approx 10^{-12}$ (spontaneous) to 10^{-13} (evoked) Tesla (6–8). These fields primarily result from a synchronized activity of postsynaptic currents in a large number of the pyramidal neurons of the cortex (14). Details about neuronal currents spatial scales are not well known. It is assumed that at least 50,000 or more cortical neurons that occupy an area of a few mm^2 must coherently act to produce magnetic fields detectable by MEG (7,8). This spatial scale is approximately that of a typical MRI voxel. The dynamic characteristics of the induced EMF and subsequently measured MEG signal have been well characterized (7,8,15,16). Relative to the stimulus onset, after a delay of about a few dozen ms a train of positive and/or negative peaks of magnetic field changes is detected. The magnetic field peak values and durations depend on stimuli type. For visual/auditory stimulations, typical ΔB peak values are on the order of $\approx 10^{-13}$ T. The typical temporal width of the ΔB peak is on the order of 100 msec. In the brain, at the current source (with measurements distance

[1]3 Tesla Functional Neuroimaging Facility, National Institute of Mental Health, NIH, Bethesda Maryland.

[2]Unit on Functional Imaging Methods, Laboratory of Brain and Cognition, National Institute of Mental Health, NIH, Bethesda Maryland.

*Correspondence to: Jerzy Bodurka, Ph.D., 3 Tesla Functional Neuroimaging Facility, National Institute of Mental Health, NIH, Bldg. 10, Rm 1D80, 10 Center Dr, MSC 1148, Bethesda, MD 20892-1148. E-mail: jbodurka@codon.nih.gov

Received 13 September 2001; revised 2 January 2002; accepted 4 February 2002.

DOI 10.1002/mrm.10159

Published online in Wiley InterScience (www.interscience.wiley.com).

order of $r_{MRI} \approx 1$–2 mm) the peak value of the ΔB (approximately scaled as $(r_{MEG}/r_{MRI})^2 \approx 10^3$ (17)) should be significantly larger. Calculations suggest that current sources causing these EMFs, assuming an approximate MRI scale of 1–2 mm, could create local peak ΔB changes on the order of 10^{-9} to 10^{-10} T lasting for less than 100 msec (8,17).

The primary motivations of this study were to 1) demonstrate a new MRI-based methodology for detection of weak and transient changes in magnetic field, $\Delta B_0(t)$; and 2) determine if the physiologically relevant transient fields on the order of 10^{-10} T and lasting for a few dozen msec are detectable by MRI.

We designed and tested a method based on a simple single-shot spin-echo (SE) echo-planar sequence (EPI) to selectively detect transient (<50 ms) changes in ΔB_0 and to suppress slow (>50 ms) changes in ΔB_0. The sensitivity of SE to transient magnetic field changes is based on the temporal placement of the 180° refocusing pulse. All $\Delta B_0(t)$ that change at a slower time than the echo time (i.e., changes in B_0 related to respiration) are refocused, but B_0 changes that happen during the time between the excitation and 180 pulse or the 180 pulse and the readout are not refocused and appear as phase shifts (18). Additionally, of course, temporal averaging of time-locked stimuli improves sensitivity. Therefore, a stable and precise synchronization between the MRI scanner and the stimulus delivery system is needed.

To demonstrate this method we created a weak and transient spatially distributed magnetic field in the vicinity of a wire placed in a water-filled container (19). Recently, with this phantom an electric current-induced field change as small as $\Delta B_C = 2$nT at echo time 27 ms was detected (19). In that study, a single-shot GE EPI sequence was used (TR/TE = 54/27 ms). The electric current was continuously provided to the phantom with 5-sec ON and 5-sec OFF periods. In this study, with the new methodology based on SE EPI with more precisely synchronized stimuli we demonstrate the detection of transient 40-ms duration current-induced field changes as small as 200 pT. The key point that will be demonstrated is that the SE sequences are no more sensitive to B_0 shifts that occur within 30 ms than GE sequences are, but that the SE sequences are much *less* sensitive than GE sequences to B_0 shifts that happen on a slower time scale (such as BOLD-related, respiration-related, and movement-related changes), therefore enhancing the detectability of small and transient field changes.

MATERIALS AND METHODS

MRI Scanner

All experiments were performed on a 3 T General Electric (Milwaukee, WI) Horizon VH/i scanner. The scanner is equipped with whole body gradient providing 40 mT/m gradient amplitude and slew rate of 150 T/m/s. A symmetric, circular birdcage geometry RF coil (IGC Medical Advances, Milwaukee, WI) optimized for brain imaging was used.

Pulse Sequences

For rapid image localization and slice selection, a gradient echo at steady-state (SPGR) sequence was used. Properly spoiled (20) single-shot and full *k*-space gradient echo (GE), and spin echo (SE) echo-planar imaging (EPI) sequences were used for time series collection. The experimental parameters for GE and SE EPI were: image matrix = 64 × 64, FOV = 16 cm, TR = 1 sec, TE = 30 for GE, and 60 or 90 ms for SE, bandwidth ±62.5 kHz, flip angle = 90°, and slice thickness = 6 mm.

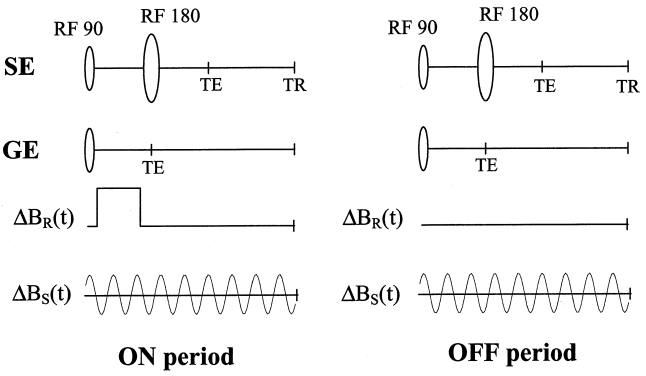

FIG. 1. Timing used in experiments. Periodic "respiration-like" magnetic field $\Delta B_S(t)$ was always present in both spin-echo (SE) and gradient echo (GE) EPI. An additional rectangular (or evoked) $\Delta B_R(t)$ transient field was only present for each TR within the ON period.

Phantom

The phantom used in measurements was described previously (19). It is composed of a glass container filled with water with a plastic frame holding two copper wires (radius = 30 μm) through which electric current can flow. The 10k resistor was connected in the series. Two pulse generators were used to provide a sinusoidal (U_S) and constant electric (U_R) voltage.

Stimulus-Scanner Synchronization

To provide the ability for stimulus generation (an electric current pulse) with controlled onset position and duration relative to a single image acquisition within the time series, a precisely synchronized stimulus delivery system was developed. The synchronization between the stimulus computer and an MRI scanner during measurement time was achieved by continuously counting triggering pulses incorporated within a pulse sequence and generated by the scanner hardware. As an example, assume that for a single-shot EPI acquisition, one trigger pulse per image located just prior to slice selection, is obtained. For p slices we have N = p pulses per TR. Therefore, within a time series lasting for t = m × TR we have N = m × p trigger pulses. The stimulus computer can generate current with controlled delay duration and amplitude relative to the trigger pulse number K (where K = 1 … N). For example, it was possible to match the onset position duration and magnitude of the rectangular electric current pulse to be located just after slice selection gradient (GE) and before 180 RF pulse (SE) in EPI (see Fig. 1). This type of stimulus is also roughly of the same dynamics as an evoked potential—essential for this simulated experiment.

Experimental Protocols

Two block design protocols were used. The first protocol consisted of three 20-sec OFF/ON epochs (120 images). Low-frequency—"respiration-like"—sinusoidal voltage changes (ν_S = 0.28 Hz and U_S = 1V or I_S = 100 μA) were always present, resulting in $\Delta B_S(t)$ of 20 nT at r = 1 mm from wire. This was used to simulate ΔB_0 changes due to respiration—*the* major obstacle in detecting small magnetic field shifts. During the ON period for each TR the additional rectangular "transient" voltage pulse (U_R = 1.5V or 0.2V) with a duration of 20 ms was generated, resulting in $\Delta B_R(t)$ of 30 nT and 4 nT, respectively, at r = 1 mm from wire. This "transient" voltage was used to simulate activation-induced current changes. The second protocol consisted of 160 repetitions of a 3-sec OFF/ON epoch (total number of images 480). In this protocol, there were no periodic $\Delta B_S(t)$. Similar to the first protocol during the rectangular transient voltage pulse (U = 0.1V or 10 μA) with a duration of 40 ms was generated (resulting in $\Delta B_R(t)$: 2 nT at r = 1 mm from wire) during the ON period. The rectangular voltage pulse position in both protocols relative to the SE and GE EPI sequence is schematically shown in Fig. 1.

Data Handling

The raw datasets in *k*-space were processed using a two-line phase reference reconstruction algorithm (21) to produce amplitude and phase images. The two reference lines were embedded into each readout window by creating one oscillation of the gradients with the y gradient "blips" off. In this manner, a unique phase reference was used for each image. This type of reconstruction is not thought to be essential for enhanced phase shift detection sensitivity. The resulting dataset consisted of N phase and amplitude images acquired from the coronal slice at equally spaced time intervals. Software for analysis, manipulation, and visualization of images included AFNI (22) and the SCILAB scientific software package (23). In every time series, the first 10 images were neglected as the MRI signal reached steady state. For each voxel the magnitude temporal signal-to-noise ratio ($TSNR_M$) was calculated. $TSNR_M$ was defined as the ratio of the average image calculated over the time course divided by the corresponding standard deviation image. $TSNR_M$ is the measurement of temporal stability and its reciprocal value determines the standard deviation (SD) of the phase noise (12,24).

RESULTS

Two experiments were conducted: 1) GE vs. SE comparison when respiration-like (sinusoidal) $\Delta B_S(t)$ and transient (rectangular) $\Delta B_R(t)$ were simultaneously present; and 2) a test for detection limit for the transient or "evoked" $\Delta B_R(t)$ field.

Results from the first experiment are summarized in Figs. 2 and 3. The bottom trace of each figure is the FFT of the phase time course from a selected pixel (white square). The upper part is the "spectral density image" at the ON/OFF switching frequency. We formed this image by choosing the switching ON/OFF (rectangular, marked by R, v = 1/40 sec = 0.025 Hz) and sinusoidal (respiration-like, marked by S, v = 0.28 Hz) frequency as a reference. The ON/OFF frequency was intentionally set at a low value similar to typical fMRI block designs. It was also our intent to demonstrate SE sensitivity to transient changes *within* these blocked runs and not to slowly changing signal drifts. First, we examined the effect of the low frequency and periodic field shifts of GE and SE data (Fig. 2). The presence of respiration-like modulation in time courses is clearly evident (S peak at 0.28 Hz). However, as expected, SE sequence compared to the GE sequence significantly reduces respiration-like phase modulation effects (Fig. 2a,b, respectively) (18). For pixels far away from the wire where the current-induced gradient is negligible, the respiration-like phase modulation is virtually removed (Fig. 2b, bottom trace). For the pixels within wire proximity (wire position marked by white arrow) the effect of the global field shift is reduced, however, with the effect of the current-induced gradient remaining (18).

Figure 3a,b shows GE data for U_R = 1.5V and 0.2V, respectively. Corresponding data for SE are shown in Fig. 3c,d, respectively. Transient magnetic field changes induced by a rectangular current pulse with amplitude 150 μA (corresponding to a field change of ΔB_R = 30 nT at the distance 1 mm from the wire) are visible both in GE and SE data (Fig. 3a,c, R peak at 0.025 Hz). Direct comparison of Fig. 3a and c shows that the SE sequence is more sensitive. If the transient voltage is reduced to 0.2V (field ≅ 4 nT, 1 mm from wire), the GE sequence is clearly less sensitive (Fig. 3b) than the SE sequence (Fig. 3d) in its detection.

Results from the second experiment are summarized in Fig. 4. This figure shows the spectral image at the ON/OFF frequency (marked by filled rectangle = 1/6 Hz). White arrows indicate wire positions. The plots show the FFT spectrum of the NMR phase time course from two pixels. The upper plot is from a voxel containing the wire indicated by the left arrow. $TSNR_M$ for this voxel was 45. The bottom plot shows the FFT spectrum from a selected voxel 12.5 mm from the left wire (indicated by a rectangle). $TSNR_M$ for this voxel was 91. It is evident that the electric current pulse with I = 10 μA and 40 ms duration-induced phase shifts are clearly detectable. Because of the larger distance between the right wire and the selected voxel, the contribution to the current-induced field shift ΔB_R in the voxel due to the right wire is negligible. Within the voxel, which contains wire, the current-induced field shift is $\Delta B_R \cong 2$ nT. The field shift in the selected voxel at the distance of x = 12.5 mm from the left wire is calculated to be $\Delta B_R \cong 0.2$ nT = 200 pT ($\Delta B_R(x,z = 0)$ is proportional to 1/x because $\Delta B_R = \mu_0/(4\pi)\, 2I\, x/(x^2 + z^2)$ (19)). Such field shift produced a well-resolved peak at the ON/OFF frequency (0.17 Hz).

DISCUSSION

In this work we introduce and demonstrate the feasibility of a new approach for MRI-based detection of ultraweak and transient magnetic field changes. The ultimate goal is the noninvasive mapping of resting and/or activation-induced neuronal activity. The key challenges are limited sensitivity, artifacts from respiration and other physiologic

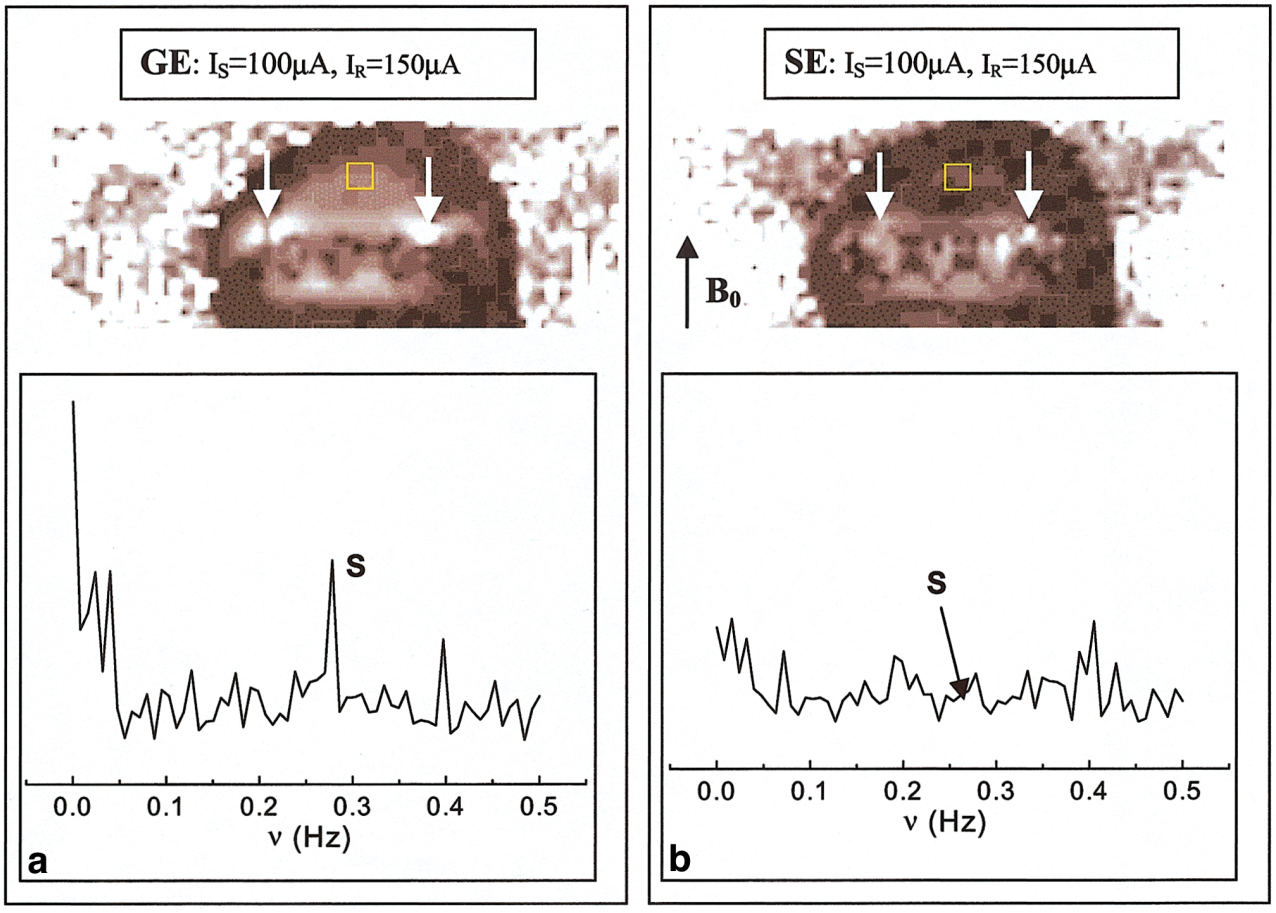

FIG. 2. Comparison of GE (**a**) and SE (**b**) sensitivity for a low-frequency (0.28 Hz) "respiration-like" (sinusoidal) electric current-induced field shift $\Delta B_S(t)$ (U_S = 1V or I_S = 100 μA, resulting in ΔB_S = 20 nT at 1 mm from wire). Upper panels are the phase spectral density images formed at the electric current frequency 0.28 Hz. Bottom traces are FFTs of a magnetic phase time course from the selected pixel (white square). Both spectra have the same scale. [Color figure can be viewed in the online issue, which is available at www.interscience.wiley.com.]

processes that can be several orders of magnitude greater than activation-induced changes, and the uncertainty regarding the magnitude and spatial/temporal heterogeneity of the current-induced changes. Lastly, depending on the precise geometry of the synchronously firing neurons, the neuronal current activity may be reflected as phase and/or magnitude changes.

If the neuron bundles are large (>100 μm) and similarly oriented, then a phase shift accompanied by a much smaller magnitude change (change in the phase dispersion) will be induced. If the bundles are more randomly distributed, then the phases will destructively add, causing minimal phase changes and greater magnitude (phase dispersion) changes. Interestingly, in this case an increase in neuronal activity would cause an increase in the ΔB_0-related phase dispersion, leading to a *decrease* in the magnitude signal during activation. Perhaps this is an alternative explanation for the "pre-undershoot" signal in BOLD contrast. In general, biocurrent patterns can be very complex due to complicated brain geometry and organization, spatial, and temporal summation of different neurons populations involved in task, and complicated regulation mechanisms (25–27). Despite all of the possible complications, MEG can detect macroscopic fields on the scalp and attribute their temporal and magnitude properties to different aspects of cognitive tasks and/or clinical disorders (7–10,15,16). From a normal, awake brain the largest (measured by MEG) magnetic field intensity order of 10^{-12} T is due to spontaneous pseudoperiodic alpha (≈10 Hz) wave activity (6,7,27). Evoked fields on the scalp due to sensory stimulations are weaker than this spontaneous activity by an order of magnitude. Their temporal pattern could be quite complicated and also irregular, showing substantial heterogeneity in relative latency and magnitude over the cortex. Within the brain a simple evaluation of the magnitude of spontaneous and evoked magnetic fields at the distance, on the order of the MRI spatial scale (single voxel size) from their current source, is in the range of 10^{-9} to 10^{-10} T (8,17). Based on data presented here, such small field changes are in the detection range of MRI. In order to detect the small magnetic phase change, SNR_M of a voxel has to be sufficiently large. The SD of the phase noise σ_ϕ is given as $\sigma_\phi \cong 1/SNR_M$ (12,24). Therefore, in order to reduce phase SD ($\Delta\sigma_\phi$) over the time course, the magnitude temporal stability ($TSNR_M$) from the given voxel should be as high as possible. $TSNR_M$ equal to 100 results in $\Delta\sigma_\phi \cong$

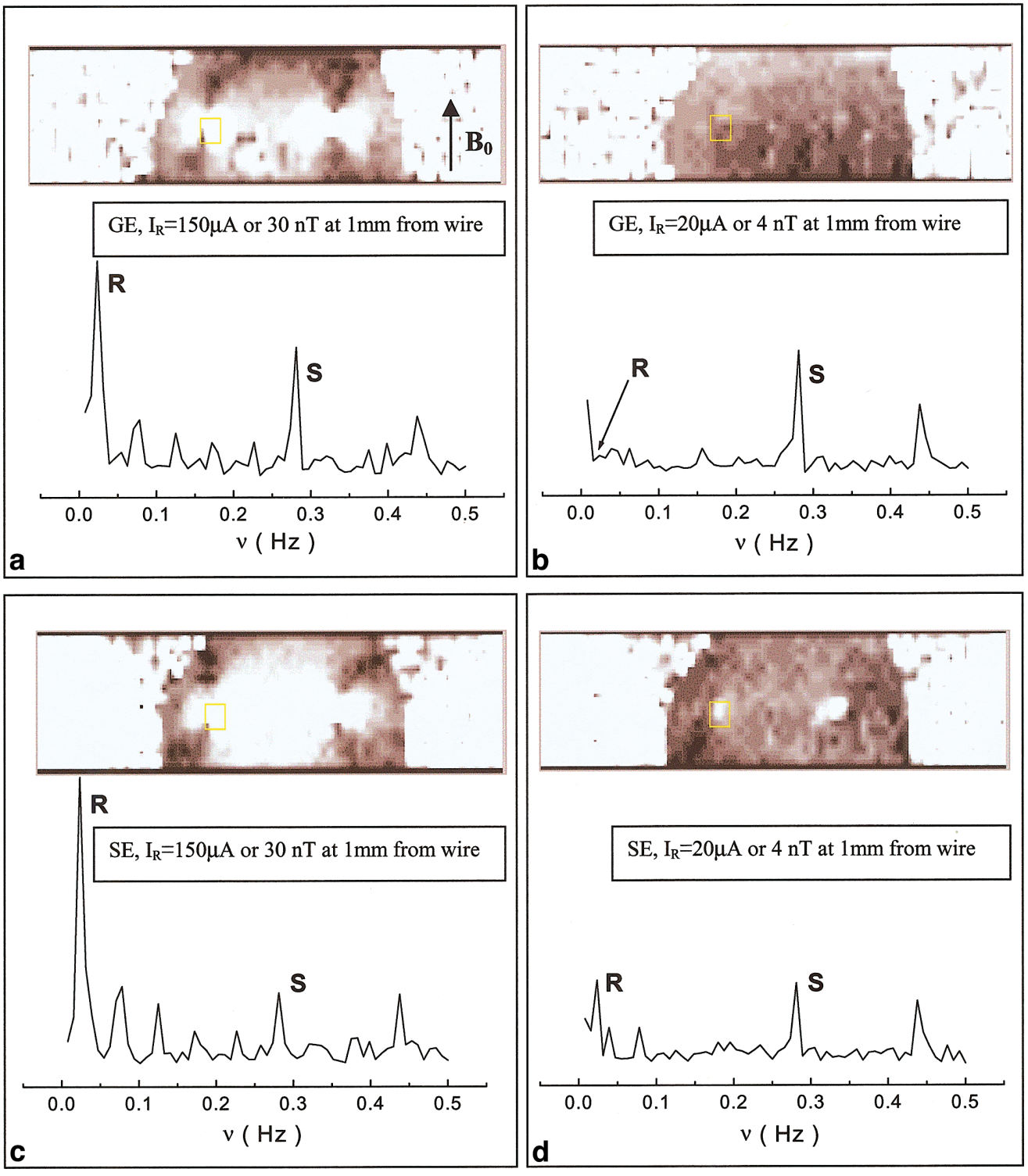

FIG. 3. Comparison of GE (**a,b**) and SE (**c,d**) EPI sensitivity for detection of the "evoked" $\Delta B_R(t)$ field. Upper panels in **a,b,c,** and **d**: the spectral images formed at 0.025 Hz (the rectangular current ON/OFF switching frequency). All spectral images are in the same scale. Bottom traces in **a,b,c,** and **d** are FFTs of a magnetic phase time course from the selected pixel (white square). All spectra are in the same scale. GE EPI data. **a:** The spectral image and FFT of the selected magnetic phase time course for the 150 μA and 20 ms duration rectangular current pulse (magnetic field of 30 nT at the distance 1 mm from the wire). R and S labels peak at the pulse ON/OFF switching and sinusoidal frequencies, respectively. **b:** The spectral image and FFT of selected pixel magnetic phase course for $U_R = 0.2V$ and 20 ms duration (resulting in $\Delta B_R \cong 4$ nT, 1 mm from wire). SE EPI data. **c:** The spectral image and FFT correspond to **a**. **d:** The spectral image and FFT correspond to **b**. GE, gradient echo, SE, spin echo, R peak at 1/40 sec = 0.025 Hz, S peak at 0.28 Hz. [Color figure can be viewed in the online issue, which is available at www.interscience.wiley.com.]

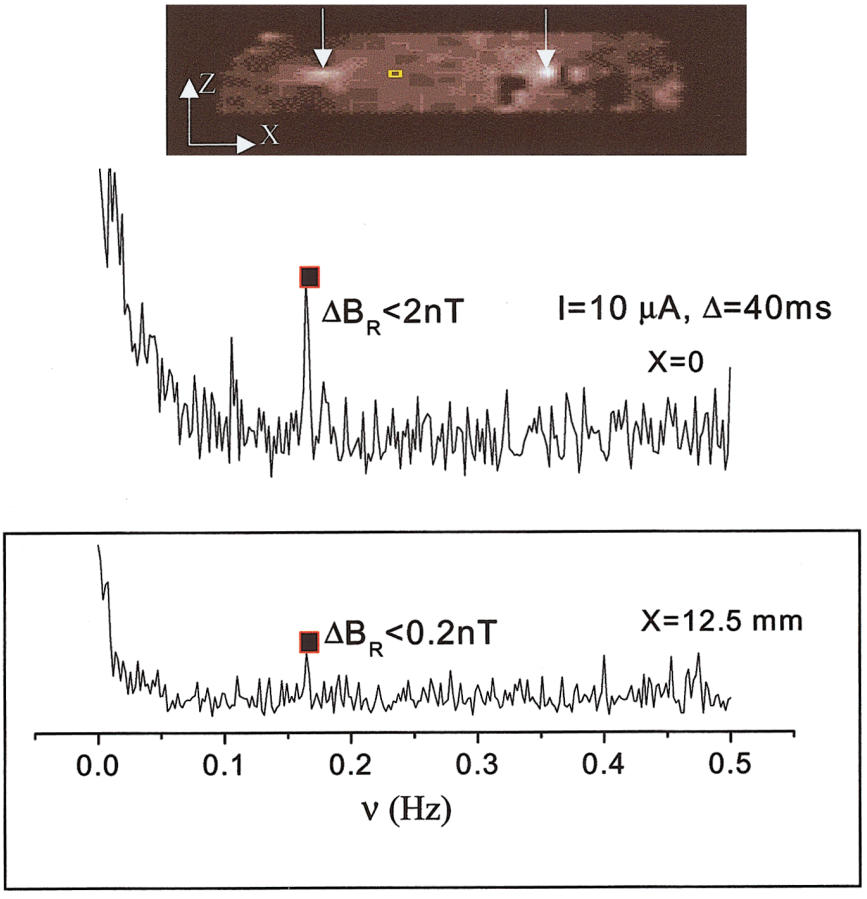

FIG. 4. Test for detection limit for rectangular and transient magnetic field $\Delta B_R(t)$. The upper panel shows the spectral image at the ON/OFF frequency (1/6 Hz and marked by a filled rectangle). The white arrows indicate wire positions. The middle panel shows FFT of the magnetic phase time course from a voxel containing the wire indicated by the left arrow. The bottom framed plot shows the FFT spectrum from a voxel 12.5 mm from the left wire (indicated by a rectangle). Within the voxel, which contains wire, the current-induced field shift is $\Delta B_R \cong 2$ nT. The field shift in the selected voxel at the distance of x = 12.5 mm from the left wire is calculated to be $\Delta B_R \cong 0.2$ nT = 200 pT. Such a field shift produced a well-resolved peak at the ON/OFF frequency (0.17 Hz). [Color figure can be viewed in the online issue, which is available at www.interscience.wiley.com.]

0.01 radians, which at echo time TE = 60 ms corresponds to $\Delta B_0(t) = 0.6$ nT. Second, the precise and consistent timing between imaging sequence and the stimulus hardware is important. A challenge to this is, of course, that while consistency in the stimulus timing is maintained, the variation and jitter of the cortical activation is perhaps more dispersed. The phase shift measured in our method is an integral value of the $\Delta B_0(t)$ over a period of time. Therefore, the temporal position of the 180 RF pulse relative to the $\Delta B_0(t)$ waveform is critical. If, for example, the evoked field is unipolar and lasts only a few dozen msec, then it should always be present immediately before, or immediately after, the 180 RF pulse. In this case, from shot-to-shot a coherent phase shift induced by this field will build up and simultaneously low-frequency unwanted field drift (like respiration) will be reduced. If these changes occur during the entire echo time or at an even distribution of times within a voxel, the effect may not be visible with this technique. These issues will certainly be explored in future work.

CONCLUSION

Transient magnetic flux density changes as small as 200 pT and lasting for 40 ms can be detected using MRI. The implications of this sensitivity are potentially significant, since approximations of field changes induced in cortex during brain activation are at this order of magnitude. While many methodological issues remain to be resolved, this work clearly indicates the potential for MRI to be used to detect and map neuronal activity directly.

ACKNOWLEDGMENTS

The authors thank Ms. Kay Kuhns for editorial assistance.

REFERENCES

1. Ogawa S, Tank DW, Menon R. Intrinsic signal changes accompanying sensor stimulation: functional brain mapping using MRI. Proc Natl Acad Sci USA 1992;89:5951–5955.
2. Bandettini PA, Wong EC, Hinks RS, Tikofsky RS, Hyde JS. Time course EPI of human brain function during task activation. Magn Reson Med 1992;25:390–397.
3. Jesmanowicz A, Bandettini P, Hyde JS. Single-shot half k-space high resolution gradient-recalled EPI for fMRI at 3 Tesla. Magn Reson Med 1998;40:754–762.
4. Menon RS, Goodyear BG. Submillimeter functional localization in human strate cortex using BOLD contrast at 4 Tesla: implications for the vascular point-spread function. Magn Reson Med 1999;41:230–235.
5. Menon RS, Luknowsky DC, Gati JS. Mental chronometry using latency-resolved functional MRI. Proc Natl Acad Sci USA 1998;95:10902–10907.
6. Cohen D. Magnetoencephalography: evidence of magnetic fields produced by alpha-rhythm currents. Science 1968;161:784–786.
7. Hamalainen M, Hari R, Ilmoniemi RJ, Knuutila J, Lounasmaa OV. Magnetoencephalography — theory, instrumentation, and applications to noninvasive studies of the working human brain. Rev Mod Phys 1993;65:413–497.
8. Romani GL. Fundamentals on neuromagnetism. In: Wiliamson S, editor. Advances in biomagnetics. New York: Plenum Press; 1989. p 33–46.

9. George JS, Aine CJ, Moshier JC, Schmidt DM, Banken DM, Schlitt HA, Wood CC, Lewine JD, Sanders JA, Belliveau JW. Mapping function in the human brain with magnetoencephalography, anatomical magnetic resonance imaging, and functional magnetic resonance imaging. J Clin Neurophysiol 1995;12:406–431.
10. Dale AM, Halgren E. Spatiotemporal mapping of brain activity by integration of multiple imaging modalities. Curr Opin Neurobiol 2000; 11:202–208.
11. Scott G, Joy M, Armstrong R, Henkelman R. RF current density imaging in homogenous media. Magn Reson Med 1992;28:186–201.
12. Scott GC, Joy MLG, Armstrong RL, Henkelman RM. Sensitivity of magnetic-resonance current-induced imaging. J Magn Reson 1992;97: 235–254.
13. Joy M, Scott G, Henkelman R. In vivo detection of applied electric currents by magnetic resonance imaging. Magn Reson Med 1989;7:89–94.
14. Humphrey DE. Re-analysis of the antidromic cortical response. II. On the contribution of cell discharge and PSPs to the evoked potentials. Electroencephalogr Clin Neurophysiol 1968;25:421–442.
15. Jousmaki V. Tracking functions of cortical networks on a milliseconds timescale. Neural Netw 2000;13:883–889.
16. Hari R, Levanen S, Raij T. Timing of human cortical functions during cognition: role of MEG. Trends Cogn Sci 2000;4:455–462.
17. Wikswo JP. Biomagnetic sources and their models. In: Wiliamson S, editor. Advances in biomagnetics. New York: Plenum Press; 1989. p 1–19.
18. Bodurka J, Zhao X, Li SJ. Analysis of physical mechanisms of respiration-induced fMRI signal changes. In: Proc 8th Annual Meeting ISMRM, Denver, 2000. p 1006.
19. Bodurka J, Jesmanowicz A, Hyde JS, Xu H, Estkowski L, Li S-J. Current-induced magnetic resonance phase imaging. J Magn Reson 1999;137: 265–271.
20. Zhao X, Bodurka J, Jesmanowicz A, Li S-J. B_0-fluctuation-induced temporal variations in EPI image series due to the disturbance of steady-state free precession (SSFP). Magn Reson Med 2000;44:758–765.
21. Jesmanowicz A, Wong EC, Hyde JS. Self-correcting EPI reconstruction algorithm. In: Proc 3rd Scientific Meeting and Exhibition SMRM, Nice, 1995. p 619.
22. Cox RW. AFNI: software for analysis and visualization of functional magnetic resonance neuroimages. Comput Biomed Res 1996;29:162–173.
23. INRIA — Unité de recherche de Rocquencourt — Projet Meta2 Domaine de Voluceau – Rocquencourt - B.P. 105 – 78153 Le Chesnay Cedex (France). The package is available at: http://www-rocq.inria.fr/scilab
24. Gudbjartsson H, Patz S. The Rician distribution of noisy MRI data. Magn Reson Med 1995;34:910–914.
25. Nunez PL. Electric field of the brain. New York: Oxford University Press; 1981.
26. Kandel E. Principles of neurosciencs. New York: McGraw-Hill; 2000.
27. Nunez PL, Wingeler BM, Silberstein RB. Spatial-temporal structures of human alpha rhythm: theory, microcurrent sources, multiscale measurements, and global binding of local networks. Hum Brain Map 2001;13:125–164.